Structural determinants of integrin β-subunit specificity for latent TGF-β

Xianchi Dong[1,2], Nathan E Hudson[1,2], Chafen Lu[1,2] & Timothy A Springer[1,2]

Eight integrin α-β heterodimers recognize ligands with an Arg-Gly-Asp (RGD) motif. However, the structural mechanism by which integrins differentiate among extracellular proteins with RGD motifs is not understood. Here, crystal structures, mutations and peptide-affinity measurements show that $\alpha_V\beta_6$ binds with high affinity to a RGDLXXL/I motif within the prodomains of TGF-β1 and TGF-β3. The LXXL/I motif forms an amphipathic α-helix that binds in a hydrophobic pocket in the β_6 subunit. Elucidation of the basis for ligand binding specificity by the integrin β subunit reveals contributions by three different βI-domain loops, which we designate specificity-determining loops (SDLs) 1, 2 and 3. Variation in a pair of single key residues in SDL1 and SDL3 correlates with the variation of the entire β subunit in integrin evolution, thus suggesting a paradigmatic role in overall β-subunit function.

Integrins are α-β heterodimers that connect diverse extracellular ligands to the cytoskeleton and regulate cell growth and differentiation[1]. The primary function of most of the 24 vertebrate integrins is to mediate cell adhesion and migration; in contrast, integrins $\alpha_V\beta_6$ and $\alpha_V\beta_8$ are specialized to activate TGF-β1 and TGF-β3 (refs. 2,3). The similarity in phenotypes of mice deficient in TGF-β1 (ref. 4) to those of mice deficient in integrin $\alpha_V\beta_6$ (ref. 2) or $\alpha_V\beta_8$ (ref. 3) and to those of mice in which RGE in latent TGF-β1 (pro-TGF-β1) has replaced RGD[5] demonstrates the importance of the RGD motif and integrins $\alpha_V\beta_6$ and $\alpha_V\beta_8$ in TGF-β1 activation *in vivo*. How integrins $\alpha_V\beta_6$ and $\alpha_V\beta_8$ achieve specificity, and how integrin β subunits in general contribute to ligand specificity, remain unclear. Little is known beyond mutational evidence for the importance of a disulfide-bonded loop (the β2-β3 loop) in the βI domain[6] and the invariant binding of the metal ion–dependent adhesion site (MIDAS) to an acidic residue present in all integrin ligands[7–10]. The issue of how the β subunit contributes specificity is particularly acute for the five RGD-recognizing integrins that contain the α_V subunit and differ only in having the β_1, β_3, β_5, β_6 or β_8 subunit.

Here, we report the molecular mechanism by which $\alpha_V\beta_6$ achieves high specificity for the RGD peptide motif present in the prodomains of TGF-β1 and TGF-β3 and the determinants of specificity for integrin β subunits in general.

RESULTS

Pro-TGF-β1 activation correlates with high integrin affinity

Transfectants expressing $\alpha_V\beta_6$ and $\alpha_V\beta_8$ but not α_V, cotransfected with the β_1, β_3 and β_5 subunits, can activate pro-TGF-β (**Fig. 1a**), results in agreement with previous studies[11]. In correlation with activation, $\alpha_V\beta_6$ and $\alpha_V\beta_8$, but not other α_V integrin transfectants, strongly bound 50 nM fluorescein isothiocyanate (FITC)-labeled pro-TGF-β1 (**Fig. 1b**).

Ligands bind to the integrin headpiece, which contains the α-subunit β-propeller domain and thigh domain as well as the β subunit βI,

hybrid, PSI and EGF1 domains. There are no previous measurements of $\alpha_V\beta_6$ affinity for ligand despite the extensive characterization of specificity and comparison among TGF-β1, TGF-β2 and TGF-β3 and among integrins in adhesion and binding assays. $\alpha_V\beta_6$ can be affinity purified with both the TGF-β1 prodomain and fibronectin[2]. Adhesion assays and enzyme-linked immunosorbent assays have indicated stronger binding of $\alpha_V\beta_6$ than $\alpha_V\beta_3$ to pro-TGF-β1 and to pro-TGF-β3 and a lack of binding in the same assays to pro-TGF-β2 (refs. 2,12). We accurately measured the affinity of monomeric pro-TGF-β3 peptide GRGDLGRL for the $\alpha_V\beta_6$ and $\alpha_V\beta_3$ headpieces with fluorescence anisotropy, using either direct binding of FITC-labeled peptide or competition with unlabeled peptide. All measurements were with the physiologic cations Mg^{2+} and Ca^{2+}. Nonapeptides containing RGD from pro-TGF-β1 and pro-TGF-β3 bound to $\alpha_V\beta_6$ with remarkably high affinity (10.3 and 8.5 nM, respectively; **Fig. 1c**). In contrast, the same peptides bound to $\alpha_V\beta_3$ with 1,000-fold-lower affinity (**Fig. 1d**). Interestingly, the homologous peptide from pro-TGF-β2, which has SGD in place of RGD, also bound to $\alpha_V\beta_6$ but with a 1,000-fold-lower affinity (8.5 μM) comparable to that of the GRGDSP peptide of fibronectin (2.5 μM; **Fig. 1c**). It is quite interesting that $\alpha_V\beta_6$ binds to pro-TGF-β2 peptide with an affinity that is in a range typically found for integrin binding to biological ligands. These results suggest that further investigation is warranted of a role for integrins, possibly distinct from that of $\alpha_V\beta_6$, in the activation of pro-TGF-β2.

$\alpha_V\beta_6$ crystal structures

We turned to crystal structures to determine the basis for the unprecedented high affinity of $\alpha_V\beta_6$ for pro-TGF-β and its peptides. Crystals of the $\alpha_V\beta_6$ headpiece, with or without a pro-TGF-β3 undecapeptide soaked in, diffracted to 2.6 and 2.85 Å (**Table 1**), respectively, and contained two molecules per asymmetric unit, with almost identical structures. The headpiece adopts the closed headpiece conformation
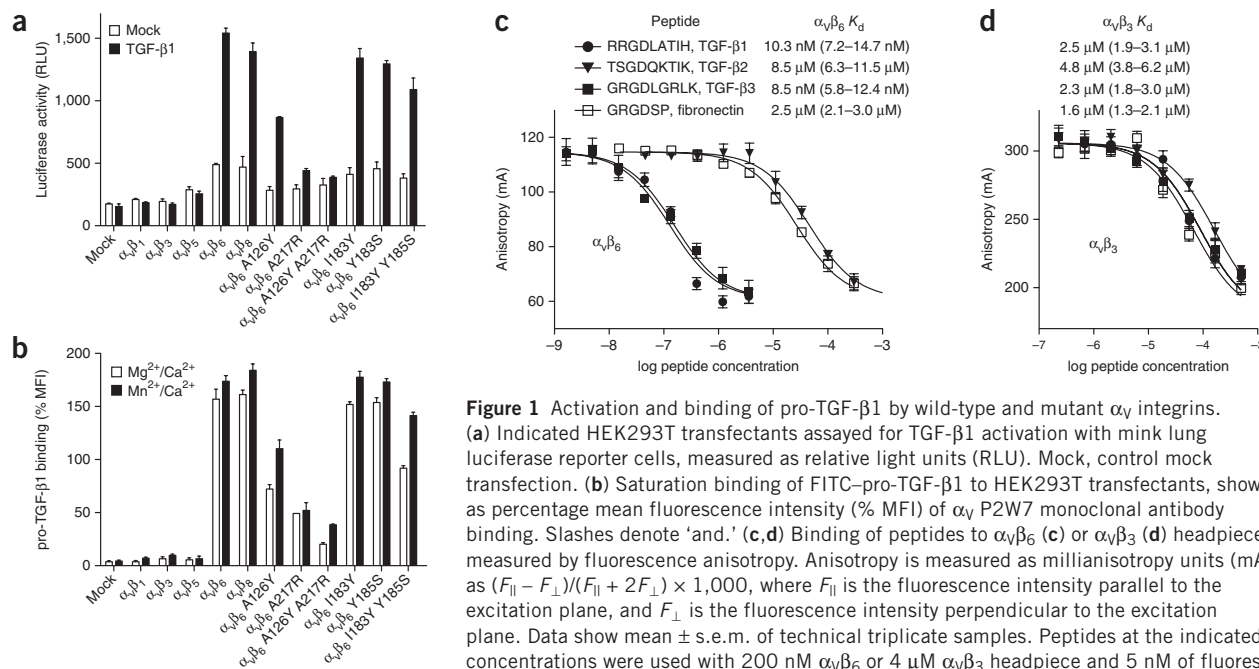
1091

Figure 1 Activation and binding of pro-TGF-β1 by wild-type and mutant α_V integrins. (**a**) Indicated HEK293T transfectants assayed for TGF-β1 activation with mink lung luciferase reporter cells, measured as relative light units (RLU). Mock, control mock transfection. (**b**) Saturation binding of FITC–pro-TGF-β1 to HEK293T transfectants, shown as percentage mean fluorescence intensity (% MFI) of α_V P2W7 monoclonal antibody binding. Slashes denote 'and.' (**c,d**) Binding of peptides to $\alpha_V\beta_6$ (**c**) or $\alpha_V\beta_3$ (**d**) headpieces, measured by fluorescence anisotropy. Anisotropy is measured as millianisotropy units (mA), as $(F_{||} - F_\perp)/(F_{||} + 2F_\perp) \times 1{,}000$, where $F_{||}$ is the fluorescence intensity parallel to the excitation plane, and $F_\perp$ is the fluorescence intensity perpendicular to the excitation plane. Data show mean ± s.e.m. of technical triplicate samples. Peptides at the indicated concentrations were used with 200 nM $\alpha_V\beta_6$ or 4 μM $\alpha_V\beta_3$ headpiece and 5 nM of fluorescent peptide probe. K_d was calculated from IC_{50} as described[30].

in the absence and presence of soaked ligand (**Fig. 2a**), i.e., with the hybrid domain swung in toward the α subunit and with the β1-α1 and β6-α7 loops and α7 helix in the βI domain in the closed

Table 1 Data collection and refinement statistics

	$\alpha_V\beta_6$	$\alpha_V\beta_6$ + TGF-β3 peptide
Data collection		
Space group	$C2$	$C2$
Cell dimensions		
a, b, c (Å)	184.5, 168.3, 101.8	184.4, 170.0, 102.4
α, β, γ (°)	90, 98.2, 90	90, 98.7, 90
Resolution (Å)	50.0–2.85 (2.95–2.85)[a]	50.0–2.60 (2.69–2.60)
R_{merge}	17.5 (349)	12.9 (198)
$I / \sigma I$	4.8 (0.4)	4.9 (0.5)
CC½ (%)[b]	98.2 (10.0)	98.8 (18.3)
Completeness (%)	97.4 (83.0)	96.4 (96.6)
Redundancy	2.4 (2.3)	2.4 (2.4)
Refinement		
Resolution (Å)	50.0–2.85	50.0–2.60
No. reflections	69,928 (4,837)	91,038 (9,101)
R_{work} / R_{free}	23.6 (38.0) / 27.9 (41.7)	21.4 (37.1) / 25.9 (37.3)
CC_{work} / CC_{free}	93.0 (29.5) / 91.0 (19.7)	94.9 (39.1) / 92.6 (27.4)
No. atoms		
Protein	16,485	16,626
Ligand/ion	– /12	166/14
Water	161	230
B factors		
Protein	96.0	76.0
Ligand/ion	– /81.5	84.7/71.9
Water	56.3	51.1
r.m.s. deviations		
Bond lengths (Å)	0.005	0.009
Bond angles (°)	0.76	1.3

[a]Values in parentheses are for highest-resolution shell. The resolution for each crystal was determined at which CC_{free} of the highest-resolution shell for the final model is about 20%.
[b]Pearson's correlation coefficient between average intensities of random half data sets for each unique reflection[31].

conformation[8,13–15]. Compared to those of β3, the βI and PSI domains of β6 are similar in structure, with greater differences in the hybrid domain (**Supplementary Table 1**).

Three closely spaced metal ion–binding sites are present in the integrin βI domain: the synergistic metal ion–binding site (SyMBS), the MIDAS and the site adjacent to the MIDAS (ADMIDAS). $\alpha_V\beta_6$ crystallized at pH 6.5 loses its SyMBS metal ion; furthermore, the SyMBS-coordinating α2-α3 loop also remodels and invades the ligand-binding pocket (**Fig. 2b**). Remodeling enables SyMBS residues Asn218 and Asp220 to point outward and to form three strong, 2.4- to 2.7-Å hydrogen bonds in place of Ca^{2+} coordination (**Fig. 2b**). Similar remodeling of the β3-subunit α2-α3 loop in the absence of a SyMBS Ca^{2+} (refs. 13,15) is blocked by the large side chains of residues that characterize its ligand-binding pocket, especially β3 Arg214 and Tyr166 in place of β6 Ala217 and Lys170 (**Fig. 2f–h**).

We hypothesized that crystallization at pH 4.5–6.5 might be responsible for variable loss of the SyMBS, MIDAS and/or ADMIDAS metal ions from $\alpha_V\beta_3$ (refs. 13,15) and $\alpha_V\beta_6$, in contrast to occupation of all three sites in $\alpha_{IIb}\beta_3$ crystalized at higher pH[14,16]. To test this hypothesis, we examined the effect of pH on affinity of $\alpha_V\beta_6$ for the TGF-β3 nonapeptide. Indeed, fluorescence anisotropy demonstrated strong pH dependence with a particularly sharp decrease in affinity between pH 7 and pH 6 (**Fig. 2c**). Because many cells coexpress integrins with their ligands, including epithelial cells that coexpress $\alpha_V\beta_6$ and pro-TGF-β1, it is possible that this pH dependence may contribute to the inhibition of ligand binding during biosynthesis in the Golgi (pH 6.0–6.7) and transport in endosomes (pH 6.3–6.5)[17].

Ligand binding by $\alpha_V\beta_6$

Soaking ligand into crystals restored a Ca^{2+}-bound conformation of the SyMBS α2-α3 loop (**Fig. 2b**) and revealed how the TGF-β3 peptide binds with high affinity (**Fig. 2d**). Simulated annealing composite omit maps show excellent ligand density (**Supplementary Fig. 1**). Ligand binding induced a local ~1.5-Å displacement of the β1-α1 loop toward the aspartate of RGD and the MIDAS Mg^{2+} (**Fig. 2b**), as seen in intermediate states of other integrins with soaked-in

RGD[7,9,13,16]. Comparing the structure of ligand-bound $\alpha_V\beta_6$ with six intermediate states of integrin $\alpha_{IIb}\beta_3$ between closed (state 1) and open (state 8), we found that the ligand-bound β_6 βI domain is similar to the intermediate state 2. In contrast, the ligand-free $\alpha_V\beta_6$ structure is clearly closed (state 1)[14,16]. The aspartate of RGD coordinated the MIDAS Mg^{2+} ion through one side chain oxygen and formed
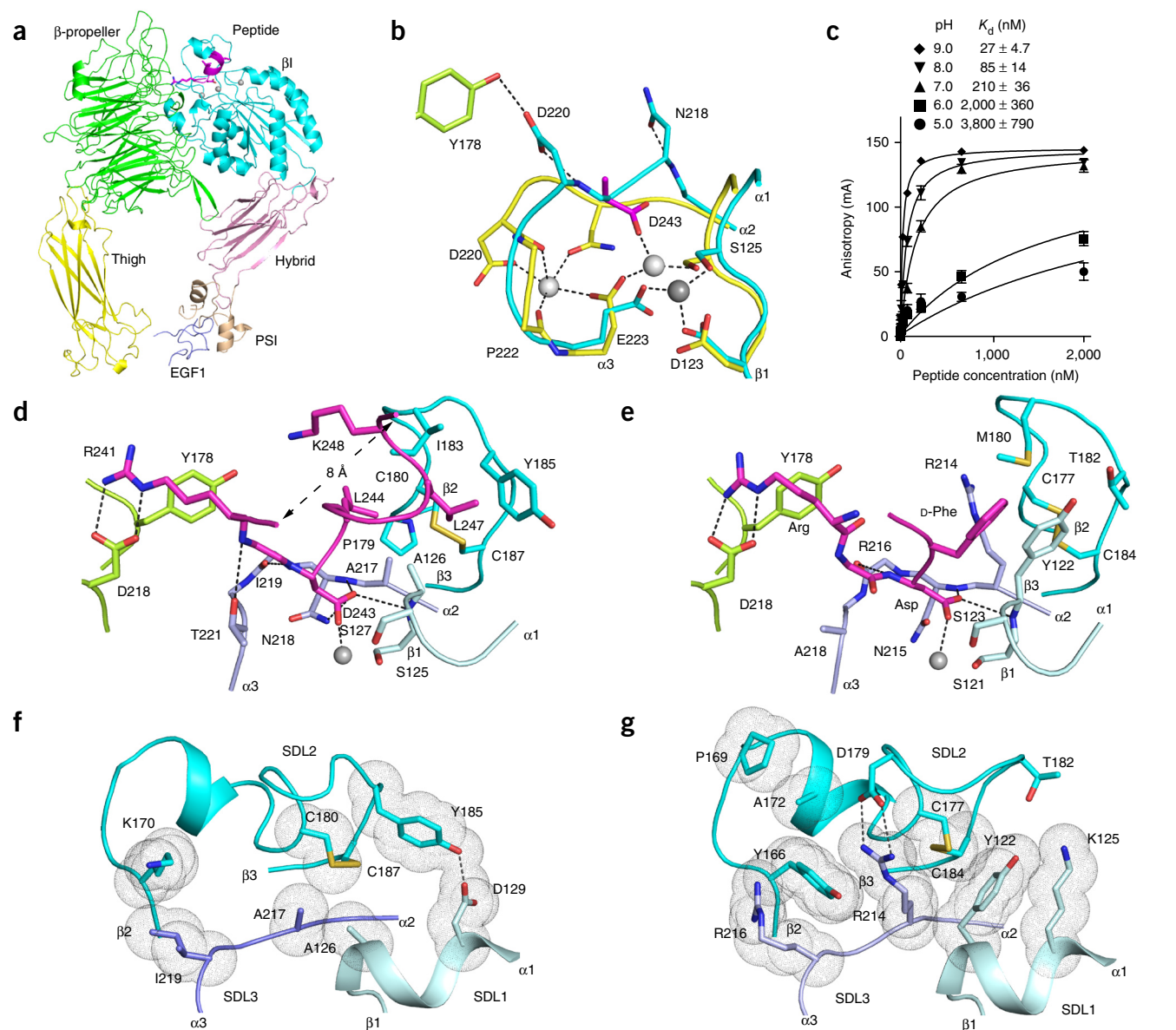
Figure 2 Crystal structures and comparisons of the $\alpha_V\beta_6$ headpiece. (**a**) Overall ribbon diagram of the $\alpha_V\beta_6$ headpiece (with each domain in a different color) with pro-TGF-$\beta3$ peptide (magenta). (**b**) Conformational change of the βI $\alpha2$-$\alpha3$ loop in the absence and presence of pro-TGF-$\beta3$. Carbon color code: green, in absence of peptide α_V; cyan, β_6; yellow, in presence of peptide β_6; magenta, peptide aspartate. Metals are white or gray spheres. (**c**) pH dependence of binding affinity. Binding of FITC–pro-TGF-$\beta3$ peptide measured with fluorescence anisotropy is shown. Data show mean ± s.e.m. of technical triplicate samples. (**d,e**) Ligand binding of $\alpha_V\beta_6$ to pro-TGF-$\beta3$ peptide (**d**) and $\alpha_V\beta_3$ to cilengitide (**e**)[7]. Carbon color code: green, α_V; cyan, β_3 or β_6, with different shades for SDLs 1, 2 and 3; magenta, ligands. The MIDAS metal ion is a silver sphere. (**f,g**) Key residues that contribute to packing between SDLs 1, 2 and 3 in β_6 (**f**) and β_3 (**g**). SDL color code is as in **d** and **e**. Van der Waals surfaces around interacting side chains are shown as dots. (**h**) Phylogenetic tree for integrin β-subunit SDL sequences[29]. Ligand-contacting residues in SDL1 and SDL3 in the X_1 positions are highlighted in pink. Residues that form packing interactions of SDL1 and SDL3 with SDL2 in the X_2 position are highlighted in orange. Cysteines forming disulfides are highlighted in yellow. Residues that coordinate metals are asterisked in orange (MIDAS), green (ADMIDAS) and cyan (SyMBS).
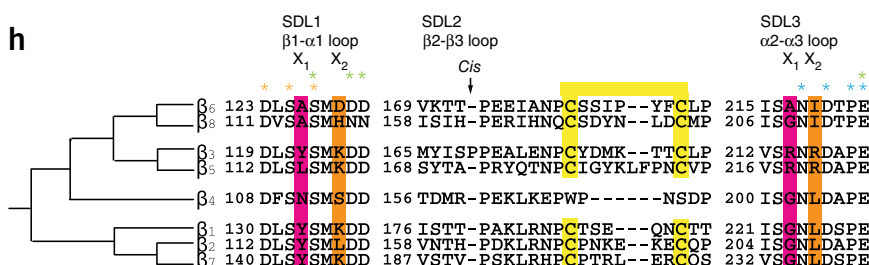
Figure 3 Ligands of $\alpha_V\beta_6$. (**a**) RGD sequences from pro-TGF-β and VP1 protein from FMDV. (**b**) Competitive binding affinities of TGF-β3 peptide truncations. Fluorescence anisotropy data are mean ± s.e.m. of technical triplicate samples scaled logarithmically. (**c**) Western blot of pro-TGF-β1 secreted by the indicated HEK293T transfectants, with antibody to the prodomain as described previously[11]. (**d**) TGF-β bioassay of pro-TGF-β1 and its double-proline mutant. Data show mean ± s.e.m. of technical triplicate samples.


hydrogen bonds to NH groups of Asn218 and Ala126 through the other side chain oxygen (**Fig. 2d**). The arginine of RGD formed bidentate hydrogen bonds through its guanido group to the side chain of Asp218 in the α_V β-propeller domain (**Fig. 2d**), as in binding to $\alpha_V\beta_3$ (**Fig. 2e**)[7]. Furthermore, as the ligand spanned the α_V-β_6 interface, the backbone of the RGD arginine formed a hydrogen bond to the side chain of Thr221 in the β_6 α2-α3 loop (**Fig. 2d**). A similar hydrogen bond to the ligand backbone can form with β_8 but not with β_3 or β_5, which have alanine in the position of β_6 Thr221 (**Fig. 2e,h**).

The largest conformational difference in the ligand-binding region between $\alpha_V\beta_6$ and $\alpha_V\beta_3$ is in the β2-β3 loop. This loop is displaced in β_6 relative to β_3 as a consequence of sequence differences in both the β2-β3 loop itself and in the β1-α1 and α2-α3 loops with which it interacts (**Fig. 2f–h**). The path of the β2-β3 loop is altered in β3 by the insertion of *cis*-Pro169 (**Fig. 2g,h**) as well as by π-cation bonds between β2-β3 residue Tyr166 and α2-α3 residues Arg214 and Arg216 (**Fig. 2g**). The three residues forming π-cation bonds are replaced in β_6 by Lys170, Ala217 and Ile219 (**Fig. 2f**). Furthermore, a hydrogen bond between Tyr185 in the β2-β3 loop and Asp129 in the β1-α1 loop constrains the conformation at the C-terminal portion of the β2-β3 loop in β_6 (**Fig. 2f**). Thus, backbone differences in the β2-β3 loop derive not only from the difference in this loop's own sequence but also from differences in the sequences of loops that interact with the β2-β3 loop.

Strikingly, the TGF-β3 peptide forms an α-helix that extensively interfaces with the β_6 subunit (**Fig. 2a,d**). Immediately following the aspartate of RGD, the sequence 244-LGRLK-248 forms an amphipathic α-helix. TGF-β Leu244 binds in a β_6-subunit hydrophobic pocket formed by the side chain of Ala217 and the backbone of Asn218 in the α2-α3 loop; the backbone of Pro179 and the side chains of Cys180 and Ile183 in the β2-β3 loop; and the side chain of Ala126 in the β1-α1 loop (**Fig. 2d**). The aliphatic portion of the ligand Lys248 side chain contributes to burying Leu244. Ligand residue Leu247 further buries Leu244 and binds in the same hydrophobic pocket by interacting with the backbone and side chain of Ala126 in the β1-α1 loop and with the side chain of Ile183, the disulfide bond of Cys177 and Cys184, and the aromatic ring of Tyr185 in the β2-β3 loop. Thus, three different loops in the βI domain make contacts with the TGF-β ligand (**Fig. 2d**).

Integrin β subunits vary markedly at the positions in the β1-α1 and α2-α3 loops where Ala126 and Ala217 contact the amphipathic TGF-β α-helix (**Fig. 2h**). Ala126, in the β_6 123-DLSAS-127 MIDAS motif, is conserved in β_8 but is a tyrosine in β_3 (Tyr122; **Fig. 2g**) and in the β_1, β_2 and β_7 subunits (**Fig. 2h**). Introduction of the tyrosine residue with the A126Y mutation substantially decreased both binding of pro-TGF-β1 and activation of TGF-β1 (**Fig. 1a,b**). Ala217 in the α2-α3 loop is a small residue (glycine or alanine) in most integrin β subunits but is a large arginine in the β_3 and β_5 subunits (**Fig. 2h**). The A217R and double A126Y A217R mutations completely abolished pro-TGF-β1 binding and activation (**Fig. 1a,b**).

Between the two disulfide-bonded cysteines in the β2-β3 loop, in which Ile183 and Tyr185 contact the pro-TGF-β α-helix, integrins are highly diverse[6] (**Fig. 2h**). However, individual β_6 I183Y and Y185S
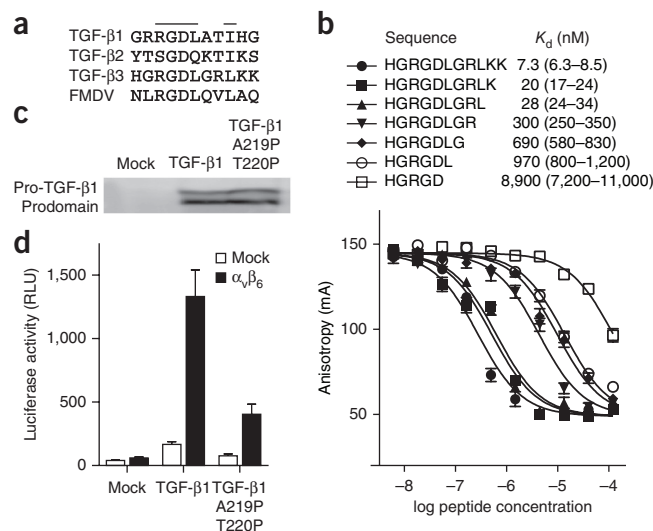
mutations had no effect, and the double mutation only slightly affected $\alpha_V\beta_6$ binding and activation of pro-TGF-β1 (**Fig. 1a,b**).

The integrin-binding loop in pro-TGF-β
In the ligand, the glycine residue preceding RGD extends back toward the amphipathic α-helix (**Fig. 2d**). Thus, Gly240 and Lys248 in 240-GRGDLGRLK-248 are only 8 Å apart (**Fig. 2d**). The sequence in between has an overall loop-like conformation, with Asp243 and Leu244 most buried in the binding pocket, which is centered on the β_6 subunit rather than the $\alpha_V\beta_6$ interface (**Fig. 2d**). Because the two ends of the pro-TGF-β3 peptide are near each another and orient away from the integrin, the peptide complex is highly compatible with integrin binding to a pro-TGF-β3 macromolecule.

The integrin-binding residues identified here lie near the middle of an 18-residue segment that is disordered or only weakly ordered in the structure of pro-TGF-β1 (ref. 18) and can easily protrude from the shoulder region of pro-TGF-β to bind $\alpha_V\beta_6$ in the helical conformation identified here. Interestingly, foot-and-mouth disease virus (FMDV) uses an RGD motif followed by an amphipathic sequence very similar to those in pro-TGF-β1 and pro-TGF-β3 (**Fig. 3a**)[19] to bind integrin $\alpha_V\beta_6$ and infect epithelial cells.

We tested the importance of the amphipathic α-helix for binding to $\alpha_V\beta_6$ by helix truncation and mutation, truncating the C terminus of the TGF-β3 undecapeptide one residue at a time (**Fig. 3b**). The largest stepwise drops in affinity, about ten-fold each, occurred when Leu244 and then Leu247 were removed (**Fig. 3b**), thus verifying the importance of these residues. To disrupt the α-helix conformation upon binding of pro-TGF-β1 to $\alpha_V\beta_6$, we mutated residues Ala220 and Thr221, which correspond to α-helix residues Gly245 and Arg246 in the pro-TGF-β3 peptide and have no contact with $\alpha_V\beta_6$, to proline. These mutations had no effect on pro-TGF-β1 expression (**Fig. 3c**), results consistent with the postulated lack of importance of this region for structural stability. However, the double-proline mutant was deficient in its ability to be activated by $\alpha_V\beta_6$ (**Fig. 3d**), thus supporting the importance of the α-helical conformation for interaction with pro-TGF-β1.

DISCUSSION
Specificity determinants of integrin β subunits
We have revealed specializations in an integrin β subunit that enable ligand recognition with high affinity and specificity. $\alpha_V\beta_6$ recognizes not only RGD but also an LXXL/I motif that folds into an amphipathic α-helix fitting into a hydrophobic pocket composed solely of residues from

the β_6 subunit. We observed these interactions with a TGF-β3 peptide bound to $\alpha_V\beta_6$ in an intermediate state. With mutations, we tested the importance of the observed interactions in binding and activation of macromolecular pro-TGF-β1 by $\alpha_V\beta_6$ on cell surfaces. These assays interrogate $\alpha_V\beta_6$ in the open conformation, because in the absence of crystal-lattice contacts, pro-TGF-β induces $\alpha_V\beta_6$ headpiece opening in the presence of Mg^{2+} and Ca^{2+} (ref. 18). Furthermore, we also measured binding in the presence of Mn^{2+}, an activator of integrin headpiece opening[20]. These results confirmed the importance of contact residues in the β1-α1 loop and α2-α3 loops in pro-TGF-β1 binding to open $\alpha_V\beta_6$. Moreover, in the βI domain's shifting to the open conformation, the α2-α3 and β2-β3 loops do not shift, and shifting in the β1-α1 loop (1.4 Å at Tyr122 in β3, equivalent to β_6 A126) is insufficient to change contact residues[8,16]. Therefore, we conclude that the observations here on β_6 residues that determine specificity for pro-TGF-β1 and pro-TGF-β3 are independent of integrin conformational state.

In contrast to our $\alpha_V\beta_6$ complex, complexes of $\alpha_V\beta_3$, $\alpha_{IIb}\beta_3$ and $\alpha_5\beta_1$ have revealed little interaction beyond that with RGD itself[7–9,16,21]. The β_6 hydrophobic-pocket interaction with the amphipathic α-helix revealed here enables $\alpha_V\beta_6$ to achieve ~1,000-fold selectivity for pro-TGF-β over the RGD motif present in fibronectin and ~1,000-fold selectivity over $\alpha_V\beta_3$ for recognition of pro-TGF-β.

The nanomolar affinity measured here is unprecedented for a monomeric integrin ligand and for a measurement in Mg^{2+} and Ca^{2+}. By comparison, RGD peptides show, in Mg^{2+} and Ca^{2+}, half-maximal effective concentration (EC_{50}) values of 7 µM to 1 mM for $\alpha_{IIb}\beta_3$ (refs. 22,23) and half-maximal inhibitory concentration (IC_{50}) values of 10–200 µM for $\alpha_{IIb}\beta_3$ (ref. 24) and 1–20 µM for $\alpha_V\beta_3$ (ref. 25). The resting affinity of integrin $\alpha_L\beta_2$ for its biological ligand is 700 µM (ref. 26). The 10-nM affinity of $\alpha_V\beta_6$ for ligand is thus unprecedented. Low integrin affinity is important to reverse adhesion in retracting regions of cells during cell migration[27]. The extraordinarily high affinity of $\alpha_V\beta_6$ may reflect a specialization to support activation of TGF-β rather than cell migration.

Previously, little had been known about the contribution of integrin β subunits to ligand recognition beyond that of the MIDAS. Our crystal structure shows that contacts with the amphipathic α-helix in the ligand, which confer high affinity for $\alpha_V\beta_6$, are mediated by the βI-domain β1-α1, β2-β3 and α2-α3 loops. Mutations demonstrated that β1-α1 and α2-α3 are important both for binding to pro-TGF-β1 and for its activation. The β2-β3 loop has previously been shown by mutation to be important for ligand selectivity by $\alpha_V\beta_3$ and $\alpha_V\beta_1$ (ref. 6) and has been designated a specificity-determining loop (SDL)[28].

We propose to designate the β1-α1, β2-β3 and α2-α3 loops SDLs 1–3, according to their order in the amino acid sequence (**Fig. 2d**–**h**). In addition to contacting the amphipathic helix, the β1-α1 (SDL1) and α2-α3 (SDL3) loops contact the glycine and aspartate of RGD. The SDL designation for the three loops in the βI domain that bind ligand is analogous to the complementarity-determining region (CDR) designation for antibody and T cell–receptor chains, which also use three surface-exposed loops to contact ligand.

In the eight human integrin β subunits, SDL1 and SDL3 have the sequences D(V/L/F)SX$_1$SMX$_2$(D/N)(D/N) and (V/I)SX$_1$NX$_2$D (A/S/T)PE, respectively (**Fig. 2h**). The two alanines in β_6 that contact pro-TGF-β are in the X$_1$ position in each loop. Variation in the X$_1$ positions of SDL1 and SDL3 correlates with variation in the entire β subunit through evolution (**Fig.(2h** and ref. 29), thus suggesting a paradigmatic role in overall β-subunit function. Thus, residues in the X$_1$ positions in SDL1 and SDL3 (respectively alanine and alanine/glycine in the β_6 and β_8 subfamily; tyrosine and glycine in the β_1, β_2 and β_7 subfamily; tyrosine/leucine and arginine in the β_3 and β_5 subfamily;

and asparagine and glycine in β_4) have a unique pattern in each subfamily, and within a subfamily variation is confined to chemically similar residues (alanine/glycine and tyrosine/leucine). Residues in the X$_2$ position in SDL1 and SDL3 pack against SDL2 and contribute to its conformational variation (**Fig. 2f**–**h**). SDL1 and SDL3 also bind metal ions (**Fig. 2h**), and thus their backbone conformations would not be free to vary unless metal ions were lost, but this loss would not be consistent with ligand binding. Switching SDL3 to a β_3-like sequence with an alanine-to-arginine substitution abolished pro-TGF-β1 binding and activation, whereas the alanine-to-tyrosine substitution in SDL1 led to partial loss of binding and activation (**Fig. 1a,b**).

As the outermost and only non-metal-binding SDL, SDL2 has a conformation that has been free to vary in evolution, as shown here in a comparison between integrins with identical α subunits, $\alpha_V\beta_3$ and $\alpha_V\beta_6$. Differences stem from the presence of a *cis*-proline in SDL2 of β_3 and packing interactions with X$_2$ residues in SDL1 and SDL3. In agreement with the lack of effect seen here of two SDL2 mutations, only one of the six residues between the two cysteines in SDL2 is identical in β_6 and β_8 (**Fig. 2h**), yet $\alpha_V\beta_6$ and $\alpha_V\beta_8$ bind and activate pro-TGF-β comparably well (**Fig. 1a,b**). This supports backbone-dependent contributions of SDL2 to integrin specificity.

Because integrins are important therapeutic targets, the identification of the three SDLs of integrin β subunits not only advances understanding of how β subunits contribute to integrin-ligand specificity but also advances the ability to rationally design antagonists.

METHODS

Methods and any associated references are available in the online version of the paper.

Accession codes. Coordinates and structure factors have been deposited in the Protein Data Bank under accession codes 4UM8 ($\alpha_V\beta_6$) and 4UM9 ($\alpha_V\beta_6$ + TGF-β3 peptide).

Note: Any Supplementary Information and Source Data files are available in the online version of the paper.

AUTHOR CONTRIBUTIONS
X.D. contributed to research design, carried out experiments, analyzed data and wrote the manuscript. N.E.H. helped to analyze the data and prepare the manuscript. C.L. contributed research design. T.A.S. conceived the experimental design, analyzed the data and wrote the manuscript.

COMPETING FINANCIAL INTERESTS
The authors declare no competing financial interests.

Reprints and permissions information is available online at http://www.nature.com/reprints/index.html.

1. Hynes, R.O. Integrins: bi-directional, allosteric, signaling machines. *Cell* **110**, 673–687 (2002).
2. Munger, J.S. *et al.* The integrin αvβ6 binds and activates latent TGFβ1: a mechanism for regulating pulmonary inflammation and fibrosis. *Cell* **96**, 319–328 (1999).
3. Mu, D. *et al.* The integrin αvβ8 mediates epithelial homeostasis through MT1-MMP-dependent activation of TGF-β1. *J. Cell Biol.* **157**, 493–507 (2002).
4. Shull, M.M. *et al.* Targeted disruption of the mouse transforming growth factor-β1 gene results in multifocal inflammatory disease. *Nature* **359**, 693–699 (1992).
5. Yang, Z. *et al.* Absence of integrin-mediated TGFβ1 activation *in vivo* recapitulates the phenotype of TGFβ1-null mice. *J. Cell Biol.* **176**, 787–793 (2007).
6. Takagi, J., Kamata, T., Meredith, J., Puzon-McLaughlin, W. & Takada, Y. Changing ligand specificities of αvβ1 and αvβ3 integrins by swapping a short diverse sequence of the β subunit. *J. Biol. Chem.* **272**, 19794–19800 (1997).
7. Xiong, J.P. *et al.* Crystal structure of the extracellular segment of integrin αVβ3 in complex with an Arg-Gly-Asp ligand. *Science* **296**, 151–155 (2002).

8. Xiao, T., Takagi, J., Wang, J.-h., Coller, B.S. & Springer, T.A. Structural basis for allostery in integrins and binding of fibrinogen-mimetic therapeutics. *Nature* **432**, 59–67 (2004).
9. Nagae, M. *et al.* Crystal structure of α5β1 integrin ectodomain: atomic details of the fibronectin receptor. *J. Cell Biol.* **197**, 131–140 (2012).
10. Sen, M., Yuki, K. & Springer, T.A. An internal ligand-bound, metastable state of a leukocyte integrin, αXβ2. *J. Cell Biol.* **203**, 629–642 (2013).
11. Wang, R. *et al.* GARP regulates the bioavailability and activation of TGF-β. *Mol. Biol. Cell* **23**, 1129–1139 (2012).
12. Ludbrook, S.B., Barry, S.T., Delves, C.J. & Horgan, C.M. The integrin αvβ3 is a receptor for the latency-associated peptides of transforming growth factors β1 and β3. *Biochem. J.* **369**, 311–318 (2003).
13. Xiong, J.-P. *et al.* Crystal structure of the extracellular segment of integrin αVβ3. *Science* **294**, 339–345 (2001).
14. Zhu, J. *et al.* Structure of a complete integrin ectodomain in a physiologic resting state and activation and deactivation by applied forces. *Mol. Cell* **32**, 849–861 (2008).
15. Dong, X. *et al.* αVβ3 integrin crystal structures and their functional implications. *Biochemistry* **51**, 8814–8828 (2012).
16. Zhu, J., Zhu, J. & Springer, T.A. Complete integrin headpiece opening in eight steps. *J. Cell Biol.* **201**, 1053–1068 (2013).
17. Paroutis, P., Touret, N. & Grinstein, S. The pH of the secretory pathway: measurement, determinants, and regulation. *Physiology (Bethesda)* **19**, 207–215 (2004).
18. Shi, M. *et al.* Latent TGF-β structure and activation. *Nature* **474**, 343–349 (2011).
19. Acharya, R. *et al.* The three-dimensional structure of foot-and-mouth disease virus at 2.9 A resolution. *Nature* **337**, 709–716 (1989).
20. Takagi, J., Petre, B.M., Walz, T. & Springer, T.A. Global conformational rearrangements in integrin extracellular domains in outside-in and inside-out signaling. *Cell* **110**, 599–611 (2002).
21. Springer, T.A., Zhu, J. & Xiao, T. Structural basis for distinctive recognition of fibrinogen γC peptide by the platelet integrin αIIbβ3. *J. Cell Biol.* **182**, 791–800 (2008).
22. Parise, L.V., Helgerson, S.L., Steiner, B., Nannizzi, L. & Phillips, D.R. Synthetic peptides derived from fibrinogen and fibronectin change the conformation of purified platelet glycoprotein IIb-IIIa. *J. Biol. Chem.* **262**, 12597–12602 (1987).
23. Frelinger, A.L. *et al.* Occupancy of an adhesive glycoprotein receptor modulates expression of an antigenic site involved in cell adhesion. *J. Biol. Chem.* **263**, 12397–12402 (1988).
24. Plow, E.F., Pierschbacher, M.D., Ruoslahti, E., Marguerie, G.A. & Ginsberg, M.H. The effect of Arg-Gly-Asp-containing peptides on fibrinogen and von Willebrand factor binding to platelets. *Proc. Natl. Acad. Sci. USA* **82**, 8057–8061 (1985).
25. Mas-Moruno, C., Rechenmacher, F. & Kessler, H. Cilengitide: the first anti-angiogenic small molecule drug candidate. Design, synthesis and clinical evaluation. *Anticancer Agents Med. Chem.* **10**, 753–768 (2010).
26. Schürpf, T. & Springer, T.A. Regulation of integrin affinity on cell surfaces. *EMBO J.* **30**, 4712–4727 (2011).
27. Springer, T.A. & Dustin, M.L. Integrin inside-out signaling and the immunological synapse. *Curr. Opin. Cell Biol.* **24**, 107–115 (2012).
28. Takagi, J., Debottis, D.P., Erickson, H.P. & Springer, T.A. The role of specificity-determining loop of the integrin β-subunit I-like domain in folding, association with the α subunit, and ligand binding. *Biochemistry* **41**, 4339–4347 (2002).
29. Huhtala, M., Heino, J., Casciari, D., de Luise, A. & Johnson, M.S. Integrin evolution: insights from ascidian and teleost fish genomes. *Matrix Biol.* **24**, 83–95 (2005).
30. Rossi, A.M. & Taylor, C.W. Analysis of protein-ligand interactions by fluorescence polarization. *Nat. Protoc.* **6**, 365–387 (2011).
31. Karplus, P.A. & Diederichs, K. Linking crystallographic model and data quality. *Science* **336**, 1030–1033 (2012).

ONLINE METHODS

Pro-TGF-β cell-surface binding and activation. α_V in a modified pEF1 vector and β_1, β_3, β_5, β_6 or β_8 mutants in pcDNA3.1 (−) vector were transiently transfected into HEK293T cells[11]. Purified pro-TGF-β1 (ref. 18) was fluorescently labeled with fluorescein isothiocyanate (FITC) with the Pierce (Thermo Fisher Scientific) FITC labeling kit according to the manufacturer's instructions. Cells were resuspended in HBS buffer (20 mM HEPES, pH 7.4, 137 mM NaCl, 5 mM KCl, 5.5 mM glucose and 1% bovine serum albumin) and incubated at room temperature for 30 min with 50 nM FITC–pro-TGF-β1 in the presence of 5 mM EDTA, 1 mM Mg^{2+}/Ca^{2+} or 1 mM Mn^{2+}/0.2 mM Ca^{2+} and subjected to flow cytometry without washing. To test the expression of different α_V integrins, cells were resuspended and incubated at room temperature for 30 min with 2 µg/ml P2W7 antibody (anti-α_V, Sigma-Aldrich, cat. no. I6778, monoclonal antibody specific for human integrin α_V (160 kDa); validation provided on the manufacturer's website) and then stained on ice for 30 min with FITC–anti-mouse IgG (1:500) (Sigma-Aldrich). Cells were washed once and subjected to fluorescence flow cytometry. Ligand binding was measured as the mean fluorescence intensity (MFI) of pro-TGF-β1 after subtraction of the MFI in the presence of EDTA.

TGF-β assays used HEK293T cells transiently transfected with the α_V and β subunits as above along with wild-type or mutant human pro-TGF-β1 in pcDNA3.1 (−) and then cocultured with transformed mink lung cells expressing a luciferase gene under the control of a TGF-β1–inducible promoter[18,32].

$\alpha_V\beta_6$ and $\alpha_V\beta_3$ headpiece expression and purification. Soluble $\alpha_V\beta_6$ headpiece was prepared similarly as in ref. 33. In brief, the α_V headpiece (residues 1–594) with the M400C mutation was followed by a 3C protease site, the ACID coiled coil, a strep II tag and a histidine tag. β_6 headpiece residues 1–474 with I270C or β_3 headpiece residues 1–472 with Q267C were followed by the 3C site, the BASE coiled coil, and a histidine tag. The cysteine mutations generated a disulfide bond that prevented α/β subunit dissociation. Proteins expressed in HEK293S GnTI⁻ cells with Ex-Cell 293 serum-free medium (Sigma) were purified with Ni-NTA affinity columns (Qiagen). Protein was cleaved by 3C protease at 4 °C overnight, passed through Ni-NTA resin and further purified with an ion-exchange gradient from 50 mM to 1 M NaCl, 20 mM Tris-HCl, pH 8.0 (Q fast-flow Sepharose, GE Healthcare) and gel filtration (Superdex 200, GE Healthcare).

Fluorescence anisotropy. Fluorescence anisotropy was in 150 mM NaCl, 1 mM Mg^{2+}/Ca^{2+}, 20 mM HEPES, pH 7.4 or buffer at the indicated pH with 5 nM fluorescence probe (FITC–pro-TGF-β3 peptide, FITC-aminohexanoic-GRGDLGRL). Binding affinities were calculated as described[30]. In saturation binding assays, the anisotropy of the fluorescence probe was measured while $\alpha_V\beta_6$ headpiece (starting at 2.67 µM) or $\alpha_V\beta_3$ headpiece (starting at 75 µM) was serially diluted in three-fold decrements. Competition binding assays used 200 nM $\alpha_V\beta_6$ or 4 µM $\alpha_V\beta_3$ headpiece, 5 nM of fluorescent probe, and competing peptide serially diluted in three-fold decrement from 500 µM to 0.5 nM.

Crystallization, data collection and structure determination. Crystals in hanging drops were formed with 3 mg/ml $\alpha_V\beta_6$ headpiece in 20 mM Tris-HCl, pH 8.0, 150 mM NaCl, 1 mM $CaCl_2$ and 1 mM $MgCl_2$ buffer (1 µl) and 1 µl reservoir solution of 20% PEG 4000, 0.1 M sodium cacodylate, pH 6.0 and 0.2 M ammonium sulfate. Identical v/v mixture of the protein and crystallization buffers yielded a pH of 6.5. Pro-TGF-β3 peptide (1 mM each Ac-HGRGDLGRLKK-NH$_2$, $MgCl_2$, and $CaCl_2$, 0.2 µl) was added to drops of ~1.5 µl (~130 µM final concentration) for 4 h before crystals were harvested. Immediately before flash freezing in liquid N$_2$, crystals were dipped in reservoir solution containing 25% glycerol with or without peptide, $MgCl_2$, and $CaCl_2$, each at 0.25 mM.

Diffraction data from GM/CA-CAT beamline 23-ID of the Advanced Photon Source (APS) at the Argonne National Laboratory were processed with XDS[34] with cross-correlation to determine the diffraction limit[31]. Structures were solved with molecular replacement by PHASER[35] with the $\alpha_V\beta_3$ headpiece from PDB 4G1E as the search model[15]. The structure was refined with PHENIX[36], manually built with Coot, and validated with MolProbity[37]. I/σI and $CC_{1/2}$ in the highest-resolution shell increase as a function of the number of diffraction images in plots generated with XDS. The resolution limit was first chosen generously on the basis of $CC_{1/2}$ of ~10% and after refinement was truncated to the resolution at which CC_{free} of the highest-resolution shell was ~20% before one final round of refinement was done at the final resolution cutoffs. Furthermore, R_{work}/R_{free} of the outer shell were 38.0%/41.7% and 36.5%/37.3% for the apo and peptide-soaked models, respectively (**Table 1**). These results show that the weak diffraction data in the outer shell contribute to structure determination. In the $\alpha_V\beta_6$-headpiece model (PDB 4UM8), 95.7%, 4.1% and 0.2% of residues have backbone dihedral angles in the favored, allowed, and outlier regions of the Ramachandran plot[37], respectively. The MolProbity[37] percentile scores are 100 and 100 for clash and geometry, respectively. In the $\alpha_V\beta_6$ headpiece TGF-β3 peptide complex model (PDB 4UM9), 95.8%, 4.1% and 0.1% of residues are in the favored, allowed and outlier Ramachandran regions, respectively and the MolProbity scores are each in the 98 percentile.

32. Abe, M. *et al.* An assay for transforming growth factor-β using cells transfected with a plasminogen activator inhibitor-1 promoter-luciferase construct. *Anal. Biochem.* **216**, 276–284 (1994).
33. Yu, Y., Schurpf, T. & Springer, T.A. How natalizumab binds and antagonizes α4 integrins. *J. Biol. Chem.* **288**, 32314–32325 (2013).
34. Kabsch, W. in *International Tables for Crystallography* Vol. F (eds Rossmann, M.G. & Arnold, E.) Ch. 25.2.9, 730–734 (Kluwer Academic Publishers, 2001).
35. McCoy, A.J. *et al.* Phaser crystallographic software. *J. Appl. Crystallogr.* **40**, 658–674 (2007).
36. Adams, P.D. *et al.* PHENIX: a comprehensive Python-based system for macromolecular structure solution. *Acta Crystallogr. D Biol. Crystallogr.* **66**, 213–221 (2010).
37. Davis, I.W. *et al.* MolProbity: all-atom contacts and structure validation for proteins and nucleic acids. *Nucleic Acids Res.* **35**, W375–W383 (2007).